Exciton-phonon coupling in diindenoperylene thin films

U. Heinemeyer,[1] R. Scholz,[2] L. Gisslén,[2] M. I. Alonso,[3] J. O. Ossó,[3,4] M. Garriga,[3] A. Hinderhofer,[1] M. Kytka,[1,5]
S. Kowarik,[1] A. Gerlach,[1] and F. Schreiber[1,*]

[1]*Institut für Angewandte Physik, Auf der Morgenstelle 10, 72076 Tübingen, Germany*
[2]*Walter Schottky Institut, Technische Universität München, Am Coulombwall 3, D-85748 Garching, Germany*
[3]*Institut de Ciència de Materials de Barcelona—CSIC, Esfera UAB, 08193 Bellaterra, Barcelona, Spain*
[4]*MATGAS 2000 A.I.E., Esfera UAB, 08193 Bellaterra, Spain*
[5]*Faculty of Electrical Engineering and Information Technology, Slovak University of Technology, Ilkovicova 3,
812 19 Bratislava, Slovakia*

We investigate exciton-phonon coupling and exciton transfer in diindenoperylene (DIP) thin films on oxidized Si substrates by analyzing the dielectric function determined by variable-angle spectroscopic ellipsometry. Since the molecules in the thin-film phase form crystallites that are randomly oriented azimuthally and highly oriented along the surface normal, DIP films exhibit strongly anisotropic optical properties with uniaxial symmetry. This anisotropy can be determined by multiple sample analysis. The thin-film spectrum is compared with a monomer spectrum in solution, which reveals similar vibronic subbands and a Huang-Rhys parameter of $S \approx 0.87$ for an effective internal vibration at $\hbar\omega_{eff}=0.17$ eV. However, employing these parameters the observed dielectric function of the DIP films cannot be described by a pure Frenkel exciton model, and the inclusion of charge-transfer (CT) states becomes mandatory. A model Hamiltonian is parametrized with density-functional theory calculations of single DIP molecules and molecule pairs in the stacking geometry of the thin-film phase, revealing the vibronic coupling constants of DIP in its excited and charged states together with electron and hole transfer integrals along the stack. From a fit of the model calculation to the observed dielectric tensor, we find the lowest CT transition E_{00}^{CT} at 0.26 ± 0.05 eV above the neutral molecular excitation energy E_{00}^{F}, which is an important parameter for device applications.

PACS number(s): 78.20.Ci, 78.66.Qn, 78.20.Bh, 71.35.Aa

I. INTRODUCTION

One of the attractive features of organic electronics and optoelectronics is the virtually unlimited choice of organic materials.[1–4] Nevertheless, a lot of attention has focused on pentacene, although this has also some shortcomings, and other materials are worth testing. Recently, diindenoperylene (DIP) has received increased attention due to its well-defined ordering, interesting growth behavior, and promising electronic transport.[5–10] In order to fully understand a material, the characterization of the optical properties is mandatory. Besides the general importance of the optical response, for organic electronics and optoelectronics the interplay between electronic and optical properties plays a key role for device performance. In addition, specifically for organic semiconductors, there are several aspects worth mentioning. Many systems exhibit a pronounced vibronic progression in the visible spectrum, allowing a direct determination of the coupling between electronic excitations and internal vibrations.[11] The coupling, frequently described by the Huang-Rhys parameter S, is given by the intensity distribution of the vibronic excitations involved. In the simplest case of a displaced harmonic oscillator, the intensities of the subbands n follow a Poisson distribution,

$$I_n = e^{-S}S^n/n! \ . \tag{1}$$

S is a relevant parameter for device applications and can be linked to the charge-carrier mobility for hopping transport.[12] Another important property is the exciton transfer in molecular aggregates, which can modify the optical spectra significantly.[13] Also anisotropy effects in phonon-assisted charge-carrier transport were reported recently.[14] In optical spectra of molecular aggregates, the oscillator strengths of electronic transitions are frequently very high and strongly anisotropic. Also, we should mention that the excitation gap as determined by optical methods may differ from the electronic gap due to a non-negligible exciton binding energy.[2]

DIP ($C_{12}H_{24}$) is a planar molecule, belonging to the point group D_{2h}. It crystallizes in two different polymorphs: a triclinic low-temperature α phase, with $Z=4$ nonplanar molecules per unit cell, and a high-temperature β phase, with a monoclinic arrangement of $Z=2$ nearly planar molecules per unit cell.[15] The thin-film phase relevant for the samples discussed here corresponds to a substrate-stabilized high-temperature phase.[5,6,15]

In this paper we present a detailed experimental and theoretical study of the optical response of DIP thin films grown by organic molecular-beam deposition (OMBD) (Refs. 3 and 4) on oxidized silicon wafers. The dielectric response including its anisotropy is determined using variable-angle spectroscopic ellipsometry (VASE).[16] Additionally, the absorption spectrum of DIP in solution is measured by UV-visible spectroscopy. The experimental data obtained in solution are interpreted using density-functional calculations of a single molecule. Based on these findings, the thin-film spectra are analyzed with two kinds of exciton models: first, a Frenkel exciton model allowing for the transfer of neutral molecular excitations between molecular sites and second an approach describing the mixing between neutral excitations and charge-transfer (CT) states. We find clear evidence that the interference between both kinds of crystal excitations is re-
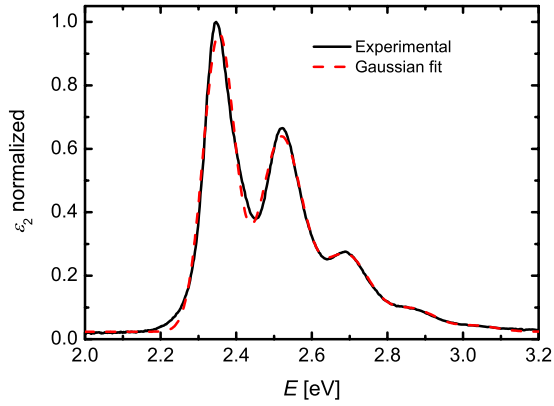
FIG. 1. (Color online) Normalized ε_2 spectrum of DIP dissolved in acetone. The experimental data [solid (black) curve] obtained from transmission measurements agree well with the fit [dashed (red)], showing a Poisson progression with a Huang-Rhys factor of $S=0.87$ for an effective mode at $\hbar\omega_{eff}=0.17$ eV, with variable Gaussian broadenings.

quired for a quantitative assignment of the observed dielectric function.

This paper is organized as follows. In Sec. II, the vibronic progression observed for dissolved (monomeric) DIP is interpreted with density-functional theory (DFT) applied to a monomer. Section III introduces spectroscopic ellipsometry and details of the data analysis applied to DIP thin films. The Frenkel exciton model is developed and compared with the experimental data in Sec. IV, followed by a discussion of possible extensions of this model in Sec. V. Section VI then describes the extended exciton model, which includes interferences between neutral and CT states. A summary and concluding remarks follow in Sec. VII.

II. SOLUTION SPECTRA (MONOMERS)

A. Experiment

In order to obtain the monomer spectrum, DIP was dissolved in acetone and the transmission intensity was measured by a Cary 50 UV-visible spectrometer. It was ensured that the concentration was sufficiently low to exclude optical nonlinearities. For solutions with low concentration, the influence of the dissolved molecules on the real part of the refractive index can be neglected and the imaginary part of the dielectric function is calculated from $\varepsilon_2=2kn_{solvent}$, where $k=\alpha 2c/\omega$ is the imaginary part of the refractive index of the molecules and $n_{solvent}=1.36$ is the refractive index of acetone.

Since the absolute numbers of the dielectric function are difficult to determine experimentally and only the relative peak heights are essential for the following analysis, the normalized ε_2 is plotted in Fig. 1 [solid (black) line], showing the highest occupied molecular orbital (HOMO)–lowest unoccupied molecular orbital (LUMO) transition, which is associated with a vibronic progression. The energy spacing is $\hbar\omega_{eff}=0.17$ eV and the intensities of the subbands can be fitted to a Poisson progression [see Eq. (1)] with variable Gaussian broadening,
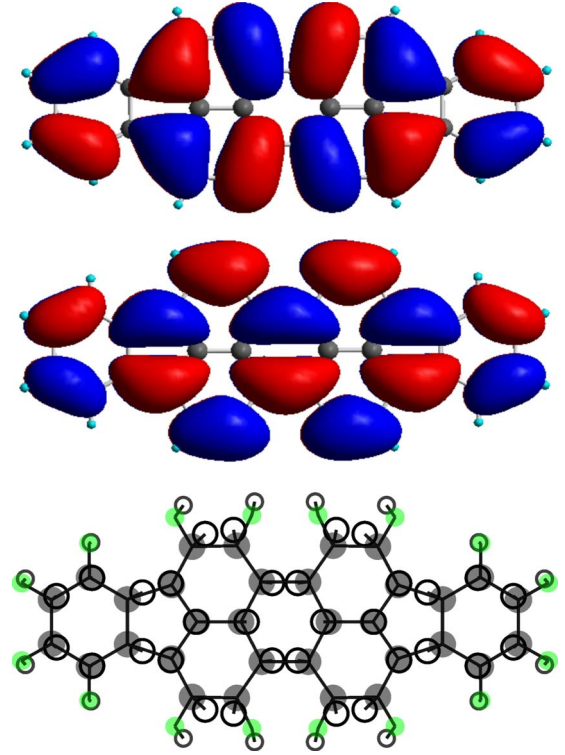

FIG. 2. (Color online) HOMO (top) and LUMO (middle) of DIP calculated with B3LYP/TZVP. Bottom: the deformation in the relaxed excited state (open circles), increased by a factor of 30, together with the relaxed ground state (solid circles).

$$\varepsilon_2 = y_0 + A_0 B_0 \sum_{i=0}^{i=4} \frac{S^i}{i\,!\,B_i} e^{-(E-E_i/B_i)^2}, \qquad (2)$$

where y_0 is some offset, A_i is the amplitude, B_i the width, and E_i the energy position of the ith Gaussian oscillator, corresponding to the 0-i transition. The effective Huang-Rhys factor is $S_{eff}=0.87$, resulting in a reorganization energy of $\lambda = S_{eff}\hbar\omega_{eff}=0.15$ eV. The 0-0 transition occurs at $E_{00}=2.35$ eV, corresponding to a vertical transition energy of $\langle E \rangle = E_{00}+\lambda=2.50$ eV in the ground-state geometry.

B. Calculated vertical transition energies

The DIP molecule has been optimized with the hybrid functional B3LYP (Refs. 17 and 18) in a triple-ζ basis set with polarization functions (TZVP) (Ref. 19) using TURBOMOLE5.7.[20] As shown in Fig. 2, the frontier orbitals are π orbitals extending over the entire molecular area, with the various lobes of the electronic wave functions typically delocalized over two neighboring carbon atoms. In this geometry, the vertical transition energies have been calculated with time-dependent (TD)-DFT (Ref. 21) (compare Table I).

In the visible, the optical properties are dominated by the HOMO-LUMO transition $1B_{1u}(x)$ at 2.347 eV with an oscillator strength of $f_{osc}=0.764$. Between the lowest transition and 4 eV, the calculation predicts some rather weak features, but above 4 eV, there are several strong transitions, all with transition dipoles along the long axis of DIP.

TABLE I. Lowest dipole-active transition energies for DIP in rectangular D_{2h} geometry. B_{1u} $\pi \rightarrow \pi^*$ transitions have their transition dipole along the long (x) axis of the molecule and B_{2u} $\pi \rightarrow \pi^*$ transitions along the short (y) axis. B_{3u} transitions with transition dipole along the molecule normal (z) do not occur in the energetic range reported. The lowest dipole-forbidden transition $1B_{1g}$ at 2.333 eV is nearly degenerate with the $1B_{1u}$ HOMO-LUMO transition.

Transition	Energy (eV)	f_{osc} (1)
$1B_{1u}(x)$	2.347	0.764
$1B_{2u}(y)$	2.970	0.001
$2B_{2u}(y)$	3.711	0.036
$2B_{1u}(x)$	3.944	0.051
$3B_{2u}(y)$	3.995	0.022
$3B_{1u}(x)$	4.220	0.587
$4B_{2u}(y)$	4.308	0.059
$4B_{1u}(x)$	4.514	0.640
$5B_{2u}(y)$	4.809	0.070
$5B_{1u}(x)$	4.908	0.321

Allowing for a typical solvent shift of −0.25 eV, the lowest calculated dipole-active $1B_{1u}$ transition would be redshifted to a vertical transition energy of about 2.1 eV in solution, 0.4 eV below the experimentally observed vertical transition energy $\langle E \rangle = 2.50$ eV. This rather small deviation indicates that gap estimates for DIP based on the hybrid functional B3LYP with its admixture of exact exchange are more reliable than pure density functionals,[22] in agreement with previous studies of transitions in aromatic molecules.[23]

In the Platt notation[24] the strong $1B_{1u}$ HOMO-LUMO transition corresponds to a ^1L_a state, whereas the weak $1B_{2u}$ (HOMO-2)-LUMO transition is denoted as ^1L_b. From a systematic TD-DFT study of various polyaromatic molecules, it is known that the B3LYP functional underestimates the energies of ^1L_a states by about 0.18 eV on average, whereas ^1L_b energies are overestimated by about 0.24 eV.[25] Therefore, it is very likely that the tabulated difference between the lowest two dipole-allowed transitions of about 0.62 eV is much too large (compare Table I).

C. Vibronic progression

The geometry of a molecule differs between different electronic configurations, e.g., between the electronic ground state and the first optically excited state. The shape of this deformation can be understood from the node patterns of the two orbitals involved in the optical transition.[26,27]

This is schematically shown in Fig. 2, where the HOMO as well as the LUMO are depicted. For bonds where a bonding region of the HOMO is replaced by an antibonding node of the LUMO, the bond length increases and vice versa.

The excited-state geometry has been optimized with two complementary methods: first, a TD-DFT optimization of the excited state and second, a constrained DFT calculation keeping the occupations $n_{\mathrm{HOMO}} = n_{\mathrm{LUMO}} = 1$ fixed. The defor-

mation pattern resulting from each of these optimizations of the excited-state geometry has been projected onto the vibrational eigenvectors calculated in the electronic ground state, revealing the Huang-Rhys factor S_j for each A_g-symmetric breathing mode $\hbar \omega_j$ together with its reorganization energy $\lambda_j = S_j \hbar \omega_j$. Even though several modes occur in the range of 0.16–0.18 eV, due to a large Gaussian broadening the progressions of these modes are not resolved in the solution spectra, resulting instead in a progression over an *effective* vibrational mode $\hbar \omega_{\mathrm{eff}}$.

In the region of interest for the observed vibronic progression, resonant Raman spectra reveal four strongly elongated modes in the range between 1289 and 1610 cm^{-1} which can all be assigned to calculated breathing modes.[28] In order to include a few smaller additional features in the theoretical analysis, we compute an effective internal vibration from an average over the elongation of internal modes in the range of 0.14–0.2 eV.

Based on this procedure and the TD-DFT geometry for the excited molecule, we find an effective Huang-Rhys factor of $S_{\mathrm{eff}} = 0.61$ and an effective mode energy of 0.174 eV (unscaled) or 0.169 eV (scaled by a prefactor of 0.973 suitable for the B3LYP functional). The effective S_{eff} obtained from TD-DFT is clearly below the observed value of 0.87. As the lowest dipole-allowed transition is dominated by a change in the occupations of HOMO and LUMO, we have performed a constrained DFT optimization of the excited geometry with fixed nonequilibrium occupation numbers, $n_{\mathrm{HOMO}} = n_{\mathrm{LUMO}} = 1$, resulting in an effective $S_{\mathrm{eff}} = 0.90$, in much better agreement with the observed solution spectra.

For ionized molecules with positive or negative charge, we find somewhat smaller deformations in the relaxed geometries, resulting in effective Huang-Rhys factors of $S_{\mathrm{eff}}^- = 0.61$ and $S_{\mathrm{eff}}^+ = 0.28$, respectively. This pronounced difference between the deformation of a molecule in an anionic and a cationic electronic configuration follows the trend observed in a large number of polyaromatic molecules, including six perylene compounds and several polyacenes. In B3LYP calculations of ionized states of polyacenes, it was found that the reorganization energies for the anionic electronic configurations were larger, but the difference with respect to cationic molecules is less pronounced.[29,30] As the deformations for excited or charged states of DIP have rather similar patterns, the exciton model discussed in Sec. IV will be based on the same effective internal vibration $\hbar \omega_{\mathrm{eff}}$ for all three patterns, involving however different Huang-Rhys factors S.

III. THIN-FILM SPECTRA

A. Sample preparation and setup

Two 1 mm thick Si(100) samples served as substrates with different oxide thicknesses. One Si substrate was thermally oxidized with a final oxide thickness of $d_{\mathrm{ThOx}} = 146$ nm and the other was covered by a native oxide ($d_{\mathrm{native}} = 1.3$ nm). Both were cleaned in an ultrasonic bath with acetone and isopropanol and then rinsed with purified water. The DIP films were grown on both substrates simultaneously by organic molecular-beam deposition under UHV

conditions at a base pressure of 2×10^{-10} mbar. The growth rate of about 2 Å/min was monitored via a water-cooled quartz-crystal microbalance (QCM). The substrate temperature was kept constant at $T = 130$ °C. For these growth conditions the crystalline structure is well ordered along the surface normal,[5] corresponding to the β phase.[15]

The VASE data were measured *ex situ* in air using a M-2000 Woollam ellipsometer in the energy range from 1.25 to 3 eV and a spectral resolution of ≈ 1.59 nm. The angle of incidence relative to the surface normal was varied in steps of 5° from $\alpha = 40° - 75°$ within a tolerance of 0.05°. Additional x-ray reflectometry data were measured with a GE/Seifert x-ray reflectometer (Cu Kα1 radiation, multilayer mirror, and double bounce compressor monochromator) in order to obtain the precise film thickness.

B. Ellipsometry data analysis

We analyze the ellipsometry data with the commercial WVASE32 software. A comparison with spectra extracted by our own β-scan program code[32] did not show any differences. The raw data consist of the ellipsometry angles Ψ and Δ that are extracted from the time-dependent detector intensity by Fourier analysis during the measurement. They are defined by the ratio of the Fresnel coefficients (see, e.g., Ref. 33),

$$\frac{r_p}{r_s} = \tan \Psi \exp(i\Delta). \tag{3}$$

A model composed of several layers with homogeneous properties and sharp interfaces was constructed in order to extract physical information about the sample (see, e.g., Refs. 33 and 34). The oxide thicknesses of the substrate were determined prior to film growth using optical functions from a database.[35]

Due to the in-plane isotropy the DIP film can be described as a uniaxial system with the optic axis perpendicular to the surface. As it is known from the literature[36–38] VASE data are not very sensitive to uniaxial anisotropy on native oxide which could be confirmed by our own measurements.[31] In order to increase the sensitivity, a multiple sample analysis was performed, where the optical functions for the DIP films on both substrates, Si with native and with thermal oxide, are coupled to be the same. This is a reasonable assumption since both films were grown simultaneously and additional AFM pictures did not show any differences in morphology. In order to exclude systematic errors and to confirm reproducibility, the analysis was repeated for several samples using either the same set of substrates or different substrates such as quartz glass. For a more detailed description of the data analysis see Ref. 31.

Prior to the ellipsometry analysis the DIP film thickness was determined by x-ray reflectometry data since the thickness analysis of the ellipsometry data alone does not give unambiguous results in this case. For samples grown on native oxide, the uniaxial anisotropy in the low absorption region is strongly correlated with layer thickness. Although this difficulty can be overcome by using the thermal oxide, slight uncertainties in the substrate model can influence the
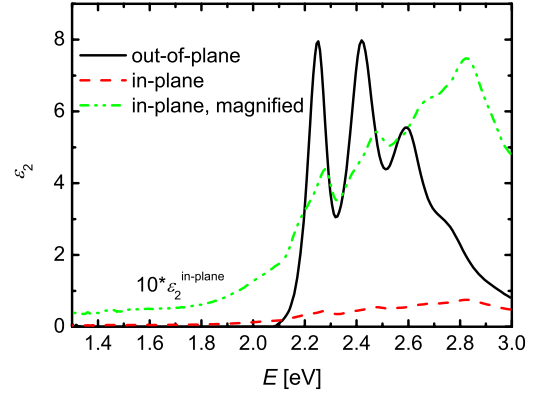

FIG. 3. (Color online) Imaginary part ε_2 for the in-plane and the out-of-plane components versus energy, obtained by a multiple sample analysis with a point-by-point fit (see text). The dash-dotted (green) curve shows the in-plane component which is magnified by a factor of 10 to better show its line shape.

film thickness as well. Therefore the film thickness on native oxide was determined by x-ray reflectometry to be $d = 33$ nm.

C. Spectra

Figures 3 and 4 show the dielectric functions ε_2 and ε_1, respectively, for the in-plane [dashed (red)] and the out-of-plane [solid (black)] components plotted as a function of energy. The results were obtained by a point-by-point fit, where the four parameters, namely, the real and the imaginary parts of the in-plane and of the out-of-plane dielectric functions, are fitted separately at each energy. An analytical fit describing the observed transitions by Gaussian oscillators was also performed and it produced nearly identical results, therefore, it is not shown here. This means that also the results of the point-by-point fit are Kramers-Kronig consistent which can also be seen by comparing ε_1 and ε_2.

The dash-dotted (green) curve in Fig. 3 shows the ε_2 in-plane component ten times magnified to better show its line shape. This difference in absolute values between both components reveals the strong uniaxial anisotropy. Furthermore,
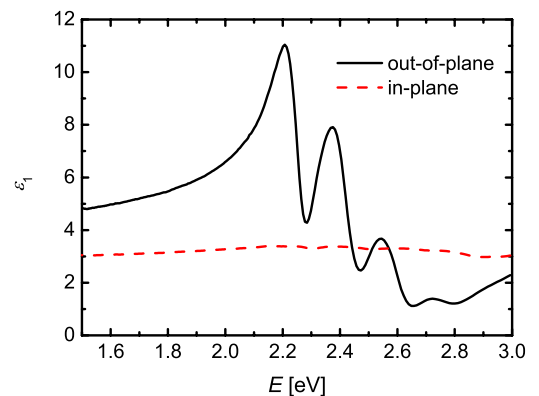

FIG. 4. (Color online) Real part ε_1 for the in-plane and the out-of-plane components versus energy, obtained by a multiple sample analysis with a point-by-point fit (see text).

both components exhibit at least four distinguishable transitions, which can be assigned to a modified vibronic progression of the HOMO-LUMO transition (see Sec. II) differing significantly between both components. While the relative intensities of the out-of-plane component rather decrease with increasing energy the in-plane component shows the opposite behavior. Also the energy positions and the spacing between the vibronic subbands differ for both directions. The effective vibronic energy of the out-of-plane component agrees with the result obtained for the monomer ($E_{01}-E_{00}$ $=0.165\pm0.005$ eV and $E_{02}-E_{01}=0.162\pm0.005$ eV), whereas the energy spacing in the in-plane component is higher ($E_{01}-E_{00}=0.202\pm0.005$ eV and $E_{02}-E_{01}$ $=0.194\pm0.005$ eV) having also a broader peak width and a different line shape, which cannot be described by a single Gaussian oscillator.

Assuming that the observed dielectric tensor arises entirely from neutral excitations of DIP molecules with transition dipole moments along their long axes, the area under the observed components of ε_2 can be used to determine the average orientation of the molecules. The tilt angle θ of the molecule relative to the surface normal can be deduced from

$$\tan^2 \theta = \frac{2I_{\text{in-plane}}}{I_{\text{out-of-plane}}}, \tag{4}$$

where I is the transition intensity given by the area under the ε_2 curves. The estimate for the tilt angle based on the lowest peak at $E_{00}=2.252$ eV gives $\theta=17°$, in excellent agreement with the published crystal structure of the thin-film phase.[15] On the other hand, due to the different line shapes between both components reported in Fig. 3, an estimate for the tilt angle based on the entire area under the curves would result in a larger tilt angle $\theta=26°$. This discrepancy indicates that a precise determination of the molecular orientation based on the imaginary part of the dielectric tensor would require an exciton model quantifying both the in-plane and the out-of-plane components.

The comparison between the thin-film spectra (Fig. 3) and the monomer spectrum (Fig. 1) shows obvious differences, such as a redshift $E_{00}^{\text{film}}-E_{00}^{\text{mono}}=-0.1$ eV for the lowest vibronic subband. This finding agrees with results of similar compounds such as PTCDA (3,4,9,10-perylene tetracarboxylic dianhydrid), where this difference is even larger (-0.16 eV). With TD-DFT methods applied to pairs of neighboring molecules in a geometry compatible with the crystalline phase of PTCDA, the contributions of different neighbors to the gas-to-crystal shift can be quantified.[39] Since the electronic transitions of the solvent, in this case acetone, are at much higher energies, their influence on the transition energies of the solute can be estimated with much simpler methods based on the refractive index in the transparent region of the solvent,[40] and usually, the gas-to-solvent shift is smaller than the gas-to-crystal shift.

With respect to the spectra in solution, the relative intensities of the vibronic subbands are changed, revealing a strong influence of the exciton transfer between different molecular sites. This will be discussed in Secs. IV and VII.

IV. FRENKEL EXCITONS

The optical properties of molecular crystals are determined by two different types of excitations: Bloch waves composed of neutral molecular excitations which are called Frenkel excitons and charge-transfer states. In the following, we will first apply a model based on Frenkel excitons, and subsequently, this approach will be extended to the mixing between Frenkel excitons and CT states. The molecular parameters S and λ related to the internal deformation are not modified with respect to the monomer spectra discussed in Sec. II, but E_{00} will be fitted to the observed dielectric function. The DIP thin-film structure used for the following calculations is taken from Ref. 15.

A. Transfer of neutral molecular excitations

The internal dynamics of each excited molecule in the crystalline phase is replaced by excitations into the different levels of a displaced harmonic oscillator for an effective internal vibration. The Franck-Condon overlap factors $S_{0_g\nu_e}$ $=\langle 0_g | \nu_e \rangle$ for such an effective mode are obtained from a Poisson progression with a fitted value of $S=0.87$ (see Sec. II). Due to the interaction between the transition dipoles on different molecules, such an excitation can be transferred to a different site,[41]

$$H^F = \sum_{\mathbf{n}\alpha\nu_e} E_{0_g\nu_e} b^\dagger_{\mathbf{n}\alpha\nu_e} b_{\mathbf{n}\alpha\nu_e} + \sum_{\mathbf{n}\alpha\nu_e} \sum_{\mathbf{m}\beta\mu_e} t_{\mathbf{n}\alpha\nu_e;\mathbf{m}\beta\mu_e} b^\dagger_{\mathbf{n}\alpha\nu_e} b_{\mathbf{m}\beta\mu_e}, \tag{5}$$

where $\mathbf{n}$ and $\mathbf{m}$ are indices for unit cells, $\alpha, \beta \in \{A, B\}$ indicate the two basis molecules, ν_e, μ_e as the indices of vibronic levels of the effective vibration, and $E_{0_g\nu_e}$ as the transition energies of the different vibronic subbands for a DIP molecule. The excitations are described by creation and annihilation operators for the vibronic level ν_e of basis molecule α in unit cell $\mathbf{n}$, $b^\dagger_{\mathbf{n}\alpha\nu_e}$ and $b_{\mathbf{n}\alpha\nu_e}$, respectively. The transfer-matrix elements $t_{\mathbf{n}\alpha\nu_e;\mathbf{m}\beta\mu_e}$ are composed of an electronic part $T_{\mathbf{n}\alpha;\mathbf{m}\beta}$ weighted with vibronic Franck-Condon factors,

$$t_{\mathbf{n}\alpha\nu_e;\mathbf{m}\beta\mu_e} = T_{\mathbf{n}\alpha;\mathbf{m}\beta} S_{0_g\nu_e} S_{0_g\mu_e}. \tag{6}$$

This approach concentrates on the states where the deformation pattern is restricted to the excited site, ignoring possible vibrational excitations on neighboring molecules. As discussed elsewhere, such states involving deformations on nonexcited sites do not carry any transition dipole, so that around $S \approx 1$ relevant for DIP, they have only a minor influence on the overall line shape.[42]

Hamiltonian (5) can be block diagonalized by a Fourier transform to the wave vector $\mathbf{k}_e$ of the Frenkel exciton,[41,43]

$$H^F(\mathbf{k}_e) = E_{0_g\nu_e} \sum_{\alpha\nu_e} b^\dagger_{\mathbf{k}_e\alpha\nu_e} b_{\mathbf{k}_e\alpha\nu_e}$$
$$+ \sum_{\alpha\nu_e} \sum_{\beta\mu_e} T_{\alpha\beta}(\mathbf{k}_e) S_{0_g\nu_e} S_{0_g\mu_e} b^\dagger_{\mathbf{k}_e\alpha\nu_e} b_{\mathbf{k}_e\beta\mu_e}, \tag{7}$$

where $T_{\alpha\beta}(\mathbf{k}_e)$ is the Fourier transform of $T_{\alpha\beta}$ in real space. The optical excitation results in an exciton state with wave vector $\mathbf{k}_e \approx 0$ in the vicinity of the Γ point of the Brillouin

zone. At $\mathbf{k}_e = 0$, the Fourier sums over the transfer-matrix elements become

$$T_{AA} = T_{AA}(0) = \sum_{\mathbf{R}_{\mathbf{n}A;\mathbf{m}A}} T_{\mathbf{n}A;\mathbf{m}A},$$

$$T_{AB} = T_{AB}(0) = \sum_{\mathbf{R}_{\mathbf{n}A;\mathbf{m}B}} T_{\mathbf{n}A;\mathbf{m}B}. \qquad (8)$$

The sum T_{AA} involving transfers toward the same basis molecule in different unit cells is dominated by the large transfer-matrix elements toward the stack neighbors, whereas the sum T_{AB} includes transfer from a reference molecule of type A toward all molecules of type B. A further block diagonalization gives the transition dipoles along two orthogonal directions defined by the sum and difference of the transition dipole moments of the two basis molecules A and B, resulting in two diagonal elements of the dielectric tensor defined with respect to these Cartesian directions.[41,43]

B. Sum rules for transition dipoles

The vibronic progression observed for such a system is subject to two types of sum rules, the first relating to the transition dipoles. If the entire absorption band arises from Frenkel excitons, its overall strength can be expressed as

$$\int dE \, \mathrm{tr}[\varepsilon_2(E)] = \frac{2\pi Z \mu^2}{\varepsilon_0 V_0}, \qquad (9)$$

where $Z = 2$ is the number of basis molecules, $V_0 = 1029$ Å^3 the volume of the crystal unit cell, and μ the transition dipole involved in the optical excitation. TD-DFT calculations of the lowest transition at the B3LYP/TZVP level define a transition dipole of $\mu = 9.42$ D $= 1.96$ eÅ, resulting in an expected area of $\int dE \, \mathrm{tr}[\varepsilon_2(E)] = 8.5$ eV. A fit of the observed dielectric function in Fig. 3 with Gaussian line shapes yields an area of only 4.2 eV, so that the experimental data result in a transition dipole of $\mu = 6.6$ D $= 1.4$ eÅ. For similar perylene compounds such as PTCDA, we have calculated a TD-DFT transition dipole of 8.25 D at the B3LYP/TZVP level, exceeding the value of 6.45 D derived from the experimental data.[44,45] Therefore, from a comparison with PTCDA, we consider the calculated transition dipole to be an upper bound, whereas the experimentally determined transition dipole rather defines a lower bound, since roughness of the film reduces the filling factor below 100%. From atomic force microscopy (AFM) and x-ray data we know that the roughness defined by the root-mean-square error of the mean film thickness is rms ≈ 4.3 nm, which is still small compared to the mean film thickness of 33 nm. Therefore, the experimental value of the transition dipole is expected to be closer to the realistic value than the calculated value.

The intensity of the two Davydov components arises from the vectorial superposition of the transition dipoles μ_A and μ_B related to the two basis molecules. Due to the small angle between the long axes of the basis molecules of only 1.4° determined by Heinrich *et al.*,[15] these transition dipoles are superimposed as $|(\mu_A + \mu_B)/\sqrt{2}| = \sqrt{2} \cos 0.7° \mu$ and $|(\mu_A - \mu_B)/\sqrt{2}| = \sqrt{2} \sin 0.7° \mu$, so that the small Davydov compo-

nent carries only a fraction of 1.5×10^{-4} of the total strength of the first absorption band. Such a tiny optical response is clearly far below the sensitivity of the ellipsometry setup, which instead probes mainly the projection of the large Davydov component into the Cartesian coordinate system defined by the orientation of the substrate plane and its normal. This assumption implies that the line shapes of the in-plane and the out-of-plane components agree, which is not the case and which will be discussed in Sec. V.

C. Sum rule for exciton transfer

In the following, the transfer-matrix element $T_{AA} + T_{AB}$ influencing the dielectric function of the dominant Davydov component will be abbreviated as T. The second kind of sum rule for Frenkel excitons relates the average transition energy $\langle E \rangle$ to a sum of molecular parameters and exciton transfer,

$$\langle E \rangle = E_{00} + S\hbar\omega + T, \qquad (10)$$

where E_{00} is the transition between the lowest vibronic levels of a molecule and $\langle E \rangle$ is the center of mass of the imaginary part of the dielectric function ε_2 in the crystalline phase.[46,47] For simplicity, we assume that the unknown gas-to-crystal shift is already lumped into the molecular parameter E_{00} used for the crystalline phase. It has to be distinguished from the lowest vibronic feature in the observed spectra because the latter relates to the lowest branch of the exciton dispersion near the Γ point of the Brillouin zone, $\mathbf{k} \approx 0$. In first-order perturbation theory, the lowest subband at Γ is expected to occur at about

$$E_{00}(\Gamma) \approx E_{00} + e^{-S} T + O(T^2). \qquad (11)$$

A more precise value is easily obtained from a diagonalization of the Hamiltonian for Frenkel excitons.[43,45] Therefore, under the simplifying assumption that the absorption line shape can be related entirely to the molecular HOMO-LUMO transition, realistic values for E_{00} and T can be read off from the energetic position of the observed peak $E_{00}(\Gamma)$ and the center of mass of ε_2.

D. Determination of transfer parameters from experiment

The next step of the analysis consists of the measurement of the center of mass of the experimental data ϵ_2 curve for the out-of-plane component. Basing the calculated center of mass on the Gaussian oscillator fit performed on the experimental data, we obtain $\langle E \rangle = 2.50 \pm 0.02$ eV. Together with a measured value $E_{00}(\Gamma) = 2.252 \pm 0.005$ eV, we can reproduce the center of mass $\langle E \rangle$ with a transfer parameter $T = 0.142$ eV and $E_{00} = 2.21$ eV, so that at Γ the excitonic dispersion shifts upward by 0.042 eV. The absolute gas-to-crystal shift of the molecular E_{00} transition is about 0.1 eV larger than the gas-to-solvent shift (compare Fig. 1), where the E_{00} band was found at 2.35 eV.

The line shape arising from the Frenkel exciton model with the above parameters is shown in Fig. 5, where the broadenings of the vibronic subbands are taken from the fit to the experimental data. The general features are qualitatively reproduced, and the calculated positions of the sub-
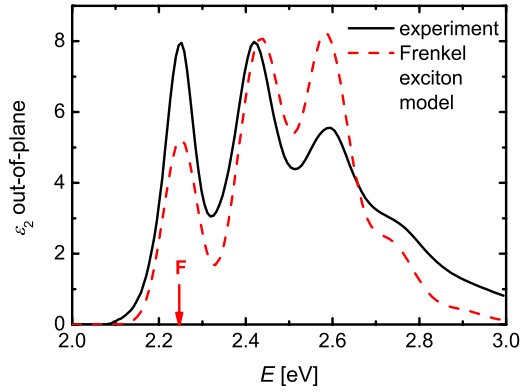
FIG. 5. (Color online) Experimental out-of-plane component ϵ_2 [solid (black)] and the result of the Frenkel exciton model [dashed (red)] with $E_{00}=2.25$ eV, $\hbar\omega_{\text{eff}}=0.17$ eV, $S=0.87$, and $T=0.142$ eV.

bands agree with the observation within absolute deviations below 0.02 eV. However, the relative intensities of the sub-bands disagree with the measured data; the central subband fits quite well, whereas the first subband at lower energies is underestimated and the third subband at higher energies is overestimated. In terms of the moments of the measured and calculated line shapes, the observed first moment $\langle E \rangle$ =2.50 eV and the measured position $E_{00}(\Gamma)=2.252$ eV were used for the definition of the model parameters, but the second moment and the related linewidth are clearly underestimated. This difference indicates additional broadening mechanisms which cannot be accounted for in this simple Frenkel exciton model.

Moreover, the relatively large transfer parameter reduces the intensity of the E_{00} subband, so that its area remains far below the observed spectra. Therefore, in the mixed Frenkel-CT model developed in Sec. VI, a smaller transfer parameter will be used, recovering a reasonable intensity of the E_{00} band. It will be shown in detail that the Frenkel-CT mixing accounts for the major part of the additional broadening of the absorption band.

V. POSSIBLE EXTENSIONS OF THE EXCITON MODEL

The fact that the shapes of the in-plane and out-of-plane components of ε_2 do not coincide indicates already that the optical response cannot arise exclusively from the large Davydov component of the Frenkel excitons based on molecular HOMO-LUMO transitions. Nevertheless, for the lowest two vibronic bands, the strength of the in-plane component corresponds to about 5% of the out-of-plane component, in good agreement with the geometric considerations in Eq. (4) related to the orientation of the molecular transition dipole and the resulting in-plane contribution of the strong Davydov component. As the small Davydov component is nearly 4 orders of magnitude smaller than the strong Davydov component, it cannot contribute a substantial fraction to the in-plane component of the dielectric tensor because a comparison of its calculated line shape with the observation would be misleading. For this reason, we do not even attempt to determine the relative size and signs of the transfer-matrix elements T_{AA} and T_{AB} defining both Davydov components.

Instead, the origin of the high energy part of the in-plane dielectric function has to be assigned to different types of transitions. A TD-DFT calculation of the lowest 16 transitions in a cluster containing two A and two B basis molecules reveals very small transition dipoles arising from CT transitions relying on the molecular HOMO and LUMO orbitals.[48] Therefore, from the weakness of the small Davydov component arising from Frenkel excitons and the absence of substantial CT dipoles involving the same orbitals, we can rule out the HOMO-LUMO transitions as a possible assignment for the upper part of the in-plane component of the dielectric tensor.

However, keeping in mind that the lowest dipole-forbidden molecular transition based on HOMO-1 and LUMO is nearly degenerate with the HOMO-LUMO transition and that the second dipole-allowed (HOMO-2)-LUMO transition is not so far higher in energy, it is clear that each of these molecular excitations generates a corresponding set of CT transitions between neighboring sites. In the cluster of four DIP molecules discussed previously, the assessment of all these transitions would require a TD-DFT calculation of the lowest 48 transitions, a task which is beyond the scope of the present analysis. From simple energetic considerations, an assignment of the upper part of the in-plane dielectric function to the orbital pairings (HOMO-2)-LUMO and (HOMO-1)-LUMO and their respective CT states seems to be the only possibility, but at the present stage, any more quantitative statements about the strength of these CT transitions would remain purely speculative.

In the following, we shall concentrate on the out-of-plane component of the dielectric tensor for which the HOMO-LUMO-based CT states modify the line shape, but the oscillator strength is still dominated by the large molecular transition dipoles of the lowest dipole-allowed excitation (compare Table I). Even though the CT transition dipoles are very small, it will be demonstrated that the shape of the dielectric function is strongly influenced by the interference between Frenkel excitons and charge-transfer transitions.

VI. MIXING OF FRENKEL EXCITONS AND CHARGE-TRANSFER STATES

A. Model Hamiltonian

The following model calculation accounts for the localized excitations visualized in Fig. 6, where the coupling between the neutral molecular excitations and the CT states is governed by the transfer parameters t_e for electrons and t_h for holes along the shortest lattice vector **a**. From a B3LYP/TZVP calculation of a stacked dimer in the geometry of the β phase of DIP,[15] these parameters can be related to the splittings of the frontier orbitals[49] $\Delta E_{\text{HOMO}}=2|t_h|$ and $\Delta E_{\text{LUMO}}=2|t_e|$ and the patterns of the resulting orbitals, giving $t_h=0.066$ eV and $t_e=-0.032$ eV. The transfer of neutral molecular excitations is described as before, and the transfer of a CT state is neglected since it would involve the simultaneous transfer of two charge carriers. For each type of
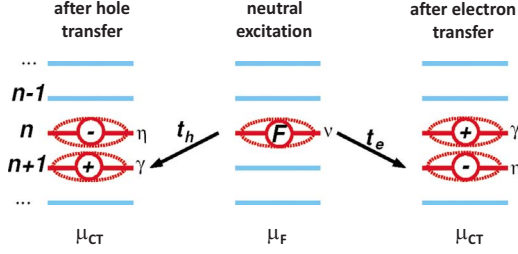
FIG. 6. (Color online) Visualization of three types of localized excited states in a stack of DIP molecules. Center: neutral molecular excitation; left: CT state obtained from the neutral excitation after transferring a hole onto the neighboring site; and right: CT state after transferring an electron. Each state can be obtained directly from the electronic ground state by an optical excitation, governed by the large transition dipole μ_F of a molecular HOMO-LUMO transition, or by the small intermolecular CT transition dipole μ_{CT}.

excitation, we account for different vibronic levels of excited or charged molecules. A similar approach for a one-dimensional stack has been applied previously to DiMe-PTCDI (dimethyl-3,4,9,10-perylene tetracarboxylic diimide) and PTCDA, but the essential parameters were not determined by DFT calculations.[42] The Hamiltonian can be divided into a part H^F for the Frenkel exciton, a part H^{CT} for the CT states, and a mixing term $H^{F\text{-}CT}$,

$$H_{\text{tot}} = H^F + H^{CT} + H^{F\text{-}CT}, \quad (12)$$

where the Frenkel part is given by Eq. (5). The second part represents the CT states involving two neighboring sites,

$$H^{CT} = E_{\gamma\eta}^{CT} \sum_{\mathbf{n}\alpha} \sum_{\gamma\eta} (c_{\mathbf{n}\alpha\gamma\eta,-1}^{\dagger} c_{\mathbf{n}\alpha\gamma\eta,-1} + c_{\mathbf{n}\alpha\gamma\eta,+1}^{\dagger} c_{\mathbf{n}\alpha\gamma\eta,+1}), \quad (13)$$

where $E_{\gamma\eta}^{CT} = E_{00}^{CT} + (\gamma + \eta)\hbar\omega_{\text{eff}}$ is the on-site energy of a CT exciton with the two molecules involved in the vibronic states γ and η of the same effective mode used for a neutral excited molecule. The operators $c_{\mathbf{n}\alpha\gamma\eta,f}^{\dagger}$ and $c_{\mathbf{n}\alpha\gamma\eta,f}$ with $f = \pm 1$ describe creation and annihilation of a CT state with an electron at lattice site $\mathbf{n}$ and a hole at the neighboring lattice site $\mathbf{n} + f\mathbf{a}$ and γ and η are the vibronic levels of the cationic and anionic molecules, respectively. Neutral excitations and CT states are mixed via

$$H^{F\text{-}CT} = \sum_{\mathbf{n}\alpha\nu} \sum_{\mathbf{m}\gamma\eta} [c_{\mathbf{m}\alpha\gamma\eta,-1}^{\dagger} b_{\mathbf{n}\alpha\nu}(\delta_{\mathbf{mn}} t_h' + \delta_{\mathbf{m},\mathbf{n}+1} t_e')$$
$$+ c_{\mathbf{m}\alpha\gamma\eta,+1}^{\dagger} b_{\mathbf{n}\alpha\nu}(\delta_{\mathbf{mn}} t_h' + \delta_{\mathbf{m},\mathbf{n}-1} t_e')] + \text{H.c.}, \quad (14)$$

with electronic transfer-matrix elements t_e' and t_h' modified by Franck-Condon factors,

$$t_e' = t_e S_{\nu_e \gamma_+} S_{0_g \eta_-}, \quad (15)$$

$$t_h' = t_h S_{0_g \gamma_+} S_{\nu_e \eta_-}, \quad (16)$$

involving each time a vibronic overlap between a charged state and a molecule in the lowest vibrational level 0 in the electronic ground state (g) and a vibronic overlap between an oppositely charged state and a neutral excited molecule (e) in the vibronic level ν, e.g., $S_{0_g \eta_-} = \langle 0_g | \eta_- \rangle$ and $S_{\nu_e \gamma_+} = \langle \nu_e | \gamma_+ \rangle$. In each case, the overlap factors account for smaller Huang-

Rhys factors of $S_{\text{eff}}^+ = 0.28$ and $S_{\text{eff}}^- = 0.61$ defined with respect to the neutral ground state, and the vibronic overlap between charged species and neutral excited molecule is defined from appropriate differences of the respective deformation patterns.

Since we have a periodic crystal, Hamiltonian (12) can again be block diagonalized by a Fourier transformation into wave-vector representation, and the sub-block for $\mathbf{k} = 0$ is diagonalized numerically.

B. Parameters for the Frenkel-CT model

In the following model calculation, the Huang-Rhys factors for an effective mode of $\hbar\omega_{\text{eff}} = 0.17$ eV are defined by their calculated B3LYP/TZVP values $S_{\text{eff}}^+ = 0.28$ and $S_{\text{eff}}^- = 0.61$ together with the fitted value $S_{\text{eff}}^e = 0.87$ obtained from dissolved DIP. The electron and hole transfer parameters $t_e = -0.032$ eV and $t_h = 0.066$ eV are obtained from a B3LYP/TZVP calculation of a stacked dimer in a geometry compatible with the high-temperature β phase of DIP, coinciding with the thin-film phase.[15] From a TD-DFT calculation of the dipole-allowed transitions in such a stacked dimer, we conclude that the transition dipole of the CT state is only about 1% of the transition dipole of a neutral molecular excitation, so that it is irrelevant for the line shape of the optical response. Instead, the large component of the observed dielectric tensor reported in Fig. 3 reveals directly the Frenkel exciton parentage of the mixed Frenkel-CT states.

The energy E_{00}^F can easily be adjusted to the measured position of the lowest structure in ε, but the transfer parameters T_{AA} and T_{AB} and the lowest level of the CT state, E_{00}^{CT}, are not yet determined. For the transfer of neutral excitations, we found that a sum of $T_{AA} + T_{AB} = 0.09$ eV is reasonable, irrespective of the assignment to the amount of exciton transfer T_{AA} between the same basis molecules and the transfer T_{AB} between different basis molecules, which is difficult to determine (see Sec. V). The transfer parameter remains smaller than the value derived from the sum rule in Sec. IV because this is the only possibility to increase the relative area of the $E_{00}(\Gamma)$ subband [compare Fig. 7(a)].

In the mixed Frenkel-CT model, the line shape at higher energies depends sensitively on the difference between Frenkel and CT energies, and the best agreement was found for $E_{00}^{CT} - E_{00}^F = 0.26$ eV or $E^{CT} = 2.50$ eV [compare Fig. 7(b)]. When performing a variation of this energy difference by ± 0.05 eV, the agreement between the model calculation and the observed line shape deteriorates significantly. From this finding, we conclude that the difference between the two types of crystal excitations is $\Delta_0 = E_{00}^{CT} - E_{00}^F = 0.26 \pm 0.05$ eV, with a rather small uncertainty. As this value is a crucial parameter for device applications such as the modulation of the optical response by applied electric fields, photocurrents, or solar cells, we consider this assignment based on optical observables to be the key achievement of the present work.

When comparing the line shape of the calculation involving only Frenkel excitons with the mixed Frenkel-CT model, the most striking difference concerns the intensity of the E_{01} subband. In our parameter set, this Frenkel subband is nearly
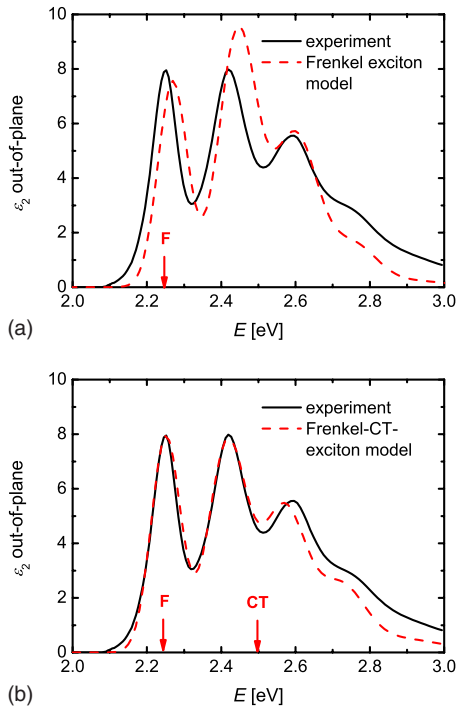
FIG. 7. (Color online) (a) Frenkel exciton model with the parameters $E_{00}^F = 2.24$ eV and $T = 0.09$ eV, which differ from those in Fig. 5. They are used for the Frenkel-CT model, shown in (b), including the interference between Frenkel and CT excitons ($E_{00}^{CT} = 2.50$ eV). The energies of the Frenkel and the CT exciton are marked by arrows.

resonant with the E_{00}^{CT} transition of the CT manifold, so that the interaction between these two excitonic features via electron and hole transfer is rather efficient. As a result, a part of the intensity of the E_{01} subband is fed into an increase in all other subbands, so that the relative height of the four largest peaks is substantially improved. A minor shortcoming of the model calculation consists in the fact that the energetic distance between the peaks $E_{01}(\Gamma)$ and $E_{02}(\Gamma)$ is underestimated by about 0.02 eV. This indicates that our Frenkel-CT model is still lacking some interaction within the exciton manifold, presumably a CT state involving the orbitals HOMO-1 or HOMO-2 or vibronic excitations on molecules surrounding the optically excited sites, as discussed previously for a purely one-dimensional system.[42]

VII. CONCLUSION

A. Solution spectrum

The solution spectrum of DIP shows a pronounced vibronic progression of the HOMO-LUMO transition which allows us to determine the Huang-Rhys parameter experimentally, giving $S = 0.87$ and a mode energy of 0.17 eV. Due to Gaussian broadening arising from the fluctuating geometry of the surroundings of each dissolved chromophore, the contributions of different internal vibrations to the vibronic subbands cannot be distinguished, so that the experimentally determined value corresponds to a sum over several internal modes. From a geometry optimization in a constrained DFT calculation using $n_{HOMO} = n_{LUMO} = 1$, we can obtain the elongation of the internal breathing modes, and a sum over the modes around 0.17 eV gives $S_{eff} = 0.90$, in good agreement with the experimental data. Furthermore, from geometry optimizations of the ionized molecule in its negative or positive charge state, we obtain effective Huang-Rhys parameters of $S_{eff}^- = 0.61$ and $S_{eff}^- = 0.28$, respectively. The reorganization energy $\lambda = 0.15$ eV for the neutral molecule and significantly smaller values for positively or negatively charged molecules are consistent with energetic trends obtained from DFT calculations for other aromatic molecules.

B. Thin-film spectra

The uniaxial optical function of DIP thin films was determined by VASE in combination with a multiple sample analysis. The type of anisotropy is consistent with our structural studies on DIP thin films on Si substrates prior to ellipsometry measurements,[5–7,9,50] showing that the molecule is standing nearly upright. Since the HOMO-LUMO transition is polarized along the long axis of the molecule, the tilt angle of the molecules relative to the surface normal can be determined to be $\theta = 17° \pm 10°$, which agrees well with single-crystal results.[15] Furthermore, from the area under the imaginary part of the dielectric tensor, we deduce a transition dipole of 6.6 D, close to the value of 6.45 D obtained from the extinction coefficient of PTCDA.

The thin-film spectrum shows a pronounced vibronic progression in both components, which differ clearly in line shape. Although the out-of-plane component agrees better with the monomer spectrum than the in-plane component, in both cases significant differences compared to the monomer spectrum can be observed, which are due to the coupling of the aggregated molecules. Since the long axes of the two basis molecules in the thin-film phase are nearly aligned, one of the two Davydov components acquires only a very small dipolar coupling strength. Therefore, this Davydov component hardly affects the in-plane component of the dielectric tensor, although it is mainly polarized along the in-plane direction of the film. Since this small component can be influenced more strongly by weak CT transitions related to (HOMO-1)-LUMO or (HOMO-2)-LUMO excitations, its computation would require a more complex exciton model. Therefore, in the theoretical analysis, we have concentrated on the strong Davydov component, thus focusing on the out-of-plane component of the dielectric function dominated by neutral molecular excitations.

Our calculations based on the results from the solution spectrum, the out-of-plane component of the thin-film spectrum, and structural properties of the thin film demonstrate that the experimental dielectric function is strongly influenced by the interference between Frenkel excitons and charge-transfer excitons. While the Frenkel exciton model alone is not sufficient to describe the experimental data, the inclusion of mixed Frenkel-CT states improves the model significantly. Based on electron and hole transfer parameters of $t_e = -0.032$ eV and $t_h = 0.066$ eV determined from DFT calculations for pairs of molecules, we can extract the difference between the excitation energy of CT and Frenkel states from the exciton model as $\Delta_0 = E_{00}^{CT} - E_{00}^F = 0.26 \pm 0.05$ eV.

*frank.schreiber@uni-tuebingen.de

[1] *Physics of Organic Semiconductors*, edited by W. Brütting (Wiley, New York, 2005).

[2] W. R. Salaneck, K. Seki, A. Kahn, and J.-J. Pireaux, *Conjugated Polymer and Molecular Interfaces: Science and Technology for Photonic and Optoelectronic Applications* (Dekker, New York, 2002).

[3] G. Witte and C. Wöll, J. Mater. Res. **19**, 1889 (2004).

[4] F. Schreiber, Phys. Status Solidi A **201**, 1037 (2004).

[5] A. C. Dürr, F. Schreiber, M. Münch, N. Karl, B. Krause, V. Kruppa, and H. Dosch, Appl. Phys. Lett. **81**, 2276 (2002).

[6] A. C. Dürr, N. Koch, M. Kelsch, A. Rühm, J. Ghijsen, R. L. Johnson, J.-J. Pireaux, J. Schwartz, F. Schreiber, H. Dosch, and A. Kahn, Phys. Rev. B **68**, 115428 (2003).

[7] A. C. Dürr, F. Schreiber, K. A. Ritley, V. Kruppa, J. Krug, H. Dosch, and B. Struth, Phys. Rev. Lett. **90**, 016104 (2003).

[8] N. Karl, *Organic Electronic Materials*, edited by R. Farchioni and G. Grosso (Springer, Berlin, 2001), p. 283.

[9] S. Kowarik, A. Gerlach, S. Sellner, F. Schreiber, L. Cavalcanti, and O. Konovalov, Phys. Rev. Lett. **96**, 125504 (2006).

[10] A. K. Tripathi and J. Pflaum, Appl. Phys. Lett. **89**, 082103 (2006).

[11] J. B. Birks, *Photophysics of Aromatic Molecules* (Wiley, New York, 1970).

[12] V. Coropceanu, J. Cornil, D. A. da Silva Filho, Y. Olivier, R. Silbey, and J. Brédas, Chem. Rev. (Washington, D.C.) **107**, 926 (2007).

[13] F. C. Spano, Annu. Rev. Phys. Chem. **57**, 217 (2006).

[14] K. Hannewald and P. A. Bobbert, Phys. Rev. B **69**, 075212 (2004).

[15] M. A. Heinrich, J. Pflaum, A. K. Tripathi, W. Frey, M. L. Steigerwald, and T. Siegrist, J. Phys. Chem. **111**, 18878 (2007).

[16] M. I. Alonso and M. Garriga, Thin Solid Films **455–456**, 124 (2004).

[17] A. D. Becke, Phys. Rev. A **38**, 3098 (1988).

[18] C. Lee, W. Yang, and R. G. Parr, Phys. Rev. B **37**, 785 (1988).

[19] A. Schäfer, C. Huber, and R. Ahlrichs, J. Chem. Phys. **100**, 5829 (1994).

[20] R. Ahlrichs, M. Bär, M. Häser, H. Horn, and C. Kölmel, Chem. Phys. Lett. **162**, 165 (1989).

[21] R. Bauernschmitt and R. Ahlrichs, J. Chem. Phys. **104**, 9047 (1996).

[22] L. M. Ramaniah and M. Boero, Phys. Rev. A **74**, 042505 (2006).

[23] M. Dierksen and S. Grimme, J. Chem. Phys. **120**, 3544 (2004).

[24] J. R. Platt, J. Chem. Phys. **17**, 484 (1949).

[25] M. Parac and S. Grimme, Chem. Phys. **292**, 11 (2003).

[26] R. Scholz, A. Y. Kobitski, T. U. Kampen, M. Schreiber, D. R. T. Zahn, G. Jungnickel, M. Elstner, M. Sternberg, and T. Frauenheim, Phys. Rev. B **61**, 13659 (2000).

[27] R. Scholz, *Encyclopedia of Condensed Matter Physics*, edited by G. Bassani, G. Liedl, and P. Wyder (Elsevier, New York, 2005), pp. 206–221.

[28] L. Gisslén *et al.* (unpublished).

[29] V. Coropceanu, M. Malagoli, D. A. da Silva Filho, N. E. Gruhn, T. G. Bill, and J. L. Brédas, Phys. Rev. Lett. **89**, 275503 (2002).

[30] V. Coropceanu, J. M. André, M. Malagoli, and J. L. Brédas, Theor. Chem. Acc. **110**, 59 (2003).

[31] U. Heinemeyer, A. Hinderhofer, M. I. Alonso, J. O. Ossó, M. Garriga, M. Kytka, A. Gerlach, and F. Schreiber, Phys. Status Solidi A **205**, 927 (2008).

[32] M. I. Alonso and M. Garriga, Thin Solid Films **455-456**, 124 (2004).

[33] R. M. A. Azzam and N. M. Bashara, *Ellipsometry and Polarized Light* (North-Holland, Amsterdam, 1977).

[34] J. Lekner, *Theory of Reflection of Electromagnetic and Particle Waves: Of Electromagnetic and Particle Waves* (Martinus Nijhoff, Dordrecht, 1987).

[35] C. M. Herzinger, B. Johs, W. A. McGahan, J. A. Woollam, and W. Paulson, J. Appl. Phys. **83**, 3323 (1998).

[36] E. G. Bortchagovsky, Thin Solid Films **307**, 192 (1997).

[37] D. J. De Smet, J. Appl. Phys. **76**, 2571 (1994).

[38] M. Campoy-Quiles, P. G. Etchegoin, and D. D. C. Bradley, Phys. Rev. B **72**, 045209 (2005).

[39] R. Scholz, A. Y. Kobitski, D. R. T. Zahn, and M. Schreiber, Phys. Rev. B **72**, 245208 (2005).

[40] N. S. Bayliss and E. G. McRae, J. Phys. Chem. **58**, 1002 (1954).

[41] A. S. Davydov, Usp. Fiziol. Nauk **82**, 393 (1964).

[42] M. Hoffmann and Z. G. Soos, Phys. Rev. B **66**, 024305 (2002).

[43] I. Vragović and R. Scholz, Phys. Rev. B **68**, 155202 (2003).

[44] A. B. Djurišić, T. Fritz, and K. Leo, Opt. Commun. **183**, 123 (2000).

[45] I. Vragović, R. Scholz, and M. Schreiber, Europhys. Lett. **57**, 288 (2002).

[46] R. Fulton and M. Gouterman, J. Chem. Phys. **41**, 2289 (1964).

[47] J. S. Briggs and A. Herzenberg, J. Phys. B **3**, 1663 (1970).

[48] TD-DFT calculation at B3LYP/DZ (double-ζ) level for a model cluster compatible with the β phase of DIP (Ref. 15).

[49] P. M. Kazmaier and R. Hoffmann, J. Am. Chem. Soc. **116**, 9684 (1994).

[50] A. C. Dürr, F. Schreiber, M. Kelsch, H. D. Carstanjen, H. Dosch, and O. H. Seeck, J. Appl. Phys. **93**, 5201 (2003).